JOURNAL OF CATALYSIS 144, 131–147 (1993)

An *in-Situ* Infrared Study of the Formation of *n*- and iso-Butyraldehyde from Propylene Hydroformylation on Rh/SiO_2 and Sulfided Rh/SiO_2

GIRISH SRINIVAS AND STEVEN S. C. CHUANG[1]

Department of Chemical Engineering, The University of Akron, Akron, Ohio 44325

Received September 9, 1992; revised June 28, 1993

In situ infrared (IR) technique has been employed to study the reaction of adsorbed CO on Rh/SiO_2 and $S–Rh/SiO_2$ with C_3H_6 and H_2, and to investigate the effect of sulfur on the *n*- and iso-butyraldehyde selectivities during steady-state propylene hydroformylation. CO adsorption on Rh/SiO_2 results in the formation of linear CO and bridged CO adsorbed on Rh^0 sites, and the gem-dicarbonyl on Rh^+ sites. CO adsorption on $S–Rh/SiO_2$ results in a high wavenumber $Rh^+(CO)$ species in addition to linear CO adsorbed on Rh^0 and the gem-dicarbonyl adsorbed on Rh^+. Sulfur decreases the rate of CO adsorption and inhibits the formation of bridged CO on Rh/SiO_2. Pulse CO chemisorption on Rh/SiO_2 and $S–Rh/SiO_2$ reveals that the equilibrium constant for CO adsorption on $S–Rh/SiO_2$ is smaller than that on Rh/SiO_2 at 303 K. Exposure of adsorbed CO to C_3H_6 at 303 K does not result in the formation of the aldehyde on both Rh/SiO_2 and $S–Rh/SiO_2$. Exposure of adsorbed CO to C_3H_6 and H_2 on Rh/SiO_2 causes a decrease in the intensity of the linear CO band and a slight increase in the intensity of the aldehyde band. A prominent decrease in the $Rh^+(CO)$ band is observed on $S–Rh/SiO_2$ with a simultaneous increase in the aldehyde band on exposure of adsorbed CO to C_3H_6 and H_2. The linear CO on Rh^+ is more active for CO insertion than linear CO on Rh^0 at 303 K. The $Rh^+(CO)$ is removed from the surface of $S–Rh/SiO_2$ at temperatures above 363 K in the presence of C_3H_6/H_2; however, the species remains stable at 513 K in the absence of H_2. Sulfided Rh/SiO_2 exhibits a higher CO insertion selectivity, a lower hydrogenation activity, and a lower n-/iso-butyraldehyde selectivity than Rh/SiO_2 during steady-state propylene hydroformylation at 513 K and 0.1–1 MPa. The analogy between homogeneous and heterogeneous hydroformylation suggests that enhancement of the isobutyraldehyde formation by adsorbed sulfur could be due to the spacious environment of the protruding Rh^+ ion sites on the $S–Rh/SiO_2$ allowing isomerization of *n*-propyl groups before CO insertion.

INTRODUCTION

Homogeneous olefin hydroformylation is a reaction of olefin with syngas that is catalyzed by Rh and Co carbonyls and their phosphine-modified complexes in organic solvent (*1–5*).The carbonyl catalysts which show high selectivity for the conversion of olefin to aldehyde under conditions as favorable as 1–2 MPa and 363–383 K have been used for commercial hydroformylation (*6*). The main disadvantage of the homogeneous process is that an energy-intensive separation stage is required to recover the catalyst from the product and solvent stream.

The heterogenization of homogeneous metal–complex catalysts has been a subject of extensive study aimed at attaching the metal complex to a carrier matrix for easy separation (*7–10*), thus combining the benefits of homogeneous and heterogeneous processes. Attempts to anchor transition metal complexes onto supports have not been very successful due to low stability of these anchored catalysts (*10*). Reaction processes using zeolite-supported Rh complexes are governed by the pore size and structure of the matrix (*11*), and reactions on oxide-supported metals yield undesired paraffin products (*10, 12*). Supported liquid (water) phase catalysts have shown promise for use as hydroformylation catalysts (*13–15*).

[1] To whom correspondence should be addressed.

0021-9517/93 $5.00

Olefin hydroformylation on supported Rh catalysts (i.e., heterogeneous hydroformylation) exhibits significantly lower selectivity to aldehyde than the homogeneous reaction catalyzed by metal carbonyls and complexes (*16–20*). Improvement of the catalyst selectivity requires fundamental understanding of the mechanism of heterogeneous hydroformylation. Recent *in situ* infrared studies have shown that single Rh^0 sites are active for ethylene hydroformylation; single Rh^+ ion sites are more active for the reaction than Rh^0 sites (*16*). Oxidation of Rh/SiO_2 causes an increase in the concentration of Rh^+ ion sites and thus an enhancement in hydroformylation activity (*16*). The addition of S and Ag to Rh/SiO_2 increases the ratio of the single Rh sites to the bridged CO sites, resulting in an improvement of the hydroformylation activity and aldehyde selectivity (*16, 17*).

Propylene hydroformylation produces both *n*-butyraldehyde and iso-butyraldehyde. An extensive compilation on homogeneous hydroformylation by Cornils (*10*) shows that the ratio of normal to iso-aldehyde is dependent on the type of ligand modifying the metal complexes, reaction temperature, and partial pressures of CO and H_2; however, little is known about the selectivity toward *n*-and iso-butyraldehyde during heterogeneous hydroformylation on Rh/SiO_2. The objectives of the present work are to study the adsorbed state of CO in a propylene hydroformylation environment and to investigate the effect of sulfur on the selectivity of *n*- and iso-butyraldehyde. A comparison is made between the effect of S on Rh/SiO_2 and the effect of phosphine ligands used in homogeneous hydroformylation catalyzed by Rh complexes.

EXPERIMENTAL

Supported rhodium catalysts containing 3 wt% Rh were prepared by impregnation of silica (large pore, Strem chemicals) with an aqueous solution of $Rh(NO_3)_3 \cdot 2H_2O$ (Alfa), using 1 cm^3 solution per g of silica. The resulting silica-supported rhodium nitrate was dried overnight in air at 313 K and reduced in flowing hydrogen (10 cm^3/min) for 16 h at 673 K. The sulfided Rh catalyst (S–Rh) was prepared by exposing the reduced catalyst to 1000 ppm H_2S in H_2 at a flow rate of 5 cm^3/min and at 673 K for 4 h. The bulk sulfur content of the S–Rh catalyst was measured by a Philips PV 9550 energy dispersive X-ray fluorescence spectrometer.

The catalyst was pressed into a self-supporting disk (10 mm in diameter, 0.5 mm in thickness) weighing 15 mg. The disk was placed in an infrared (IR) cell which consists of four stainless steel flanges and two CaF_2 step windows that minimize the IR pathlength for the gaseous species (*16*). The pathlength for the infrared beam in the cell is slightly less than 2 mm and the net reactor volume is 0.2 cm^3. The cell can be used up to 6 MPa and in the temperature range 293–533 K. Infrared spectra were obtained by a Fourier transform infrared spectrometer with a DTGS detector at a resolution of 4 cm^{-1}. Pulse CO chemisorption (*21*) in He carrier gas on Rh/SiO_2 and $S–Rh/SiO_2$ and pulse H_2 chemisorption on Rh/SiO_2 were performed at 303 K in a differential reactor and the eluted gas was analyzed by a Balzers QMG 112 mass spectrometer (MS) interfaced with a microcomputer. The amount of CO or H_2 adsorbed was determined by the difference in the amounts of CO or H_2 upstream and downstream of the reactor during each pulse. Pulse CO chemisorption measurements were further undertaken in the IR reactor cell to determine the integrated IR absorption coefficients. The same approach was used to calculate the amount of CO chemisorbed during each pulse.

Infrared study of CO adsorption was carried out by admitting CO (10 cm^3/min) into the IR reactor cell at 303 K and 0.1 MPa for 2–3 min. The catalyst was then flushed with N_2 or He (20 cm^3/min) for 5 min to remove any gaseous species before the IR spectra were taken. The reaction of adsorbed CO with C_3H_6/H_2 (or C_3H_6 only) was carried out by exposure of adsorbed CO to a mixture

of C_3H_6/H_2 = 1 : 1 (or C_3H_6 only) at 0.1 MPa. The IR spectra of the reaction of C_3H_6/H_2 with CO adsorbed on Rh/SiO_2 were taken as a function of reaction time. The same investigation was performed on the S–Rh/SiO_2 catalyst.

Steady-state propylene hydroformylation ($CO : H_2 : C_3H_6$ = 1 : 1 : 1, total flow rate = 15 cm^3/min) was performed on Rh/SiO_2 and S–Rh/SiO_2 in the IR reactor cell at 513 K and 0.1–1 MPa. Steady-state propylene hydrogenation ($C_3H_6 : H_2$ = 1 : 1, total flow rate = 10 cm^3/min) was also carried out on Rh/SiO_2 and S–Rh/SiO_2 in the IR cell at 513 K and 0.1 MPa. During all the steady-state runs, the products of the reaction were analyzed by an HP 5890A gas chromatograph with a 1.8-m Poropak PS column in series with a 1.8-m Poropak QS column. The temperature programming of the column was as follows: 313 to 383 K in 7 min, 383 to 473 K in 45 min, and maintaining at 473 K for 8 min, which provided a good separation of C_1–C_6 olefins and paraffins, and C_1–C_4 aldehydes and alcohols.

RESULTS

CO Adsorption on Rh/SiO_2 and S–Rh/SiO_2

Figure 1 shows the IR spectra of CO adsorbed on Rh/SiO_2 and sulfided Rh/SiO_2. Two intense bands, linearly adsorbed CO at 2070 cm^{-1} and bridged CO at 1894 cm^{-1}, were observed on the Rh/SiO_2 catalyst. A small band at 2102 cm^{-1} and a shoulder at 2036 cm^{-1} have been ascribed to the symmetrical and asymmetrical stretching modes of $Rh^+(CO)_2$, the gem-dicarbonyl species. These assignments are in agreement with those in literature (*16, 17, 19, 22–31*).

CO adsorption on sulfided Rh/SiO_2 gave rise to the following: (a) a linear CO band at 2073 cm^{-1}, (b) a weak bridged CO band at 1873 cm^{-1}, (c) the asymmetric gem-dicarbonyl band at 2031 cm^{-1} whose intensity remained about the same as that observed on the Rh/SiO_2, and (d) an intense band at 2095 cm^{-1}. The unusually high ratio of intensity of the band at 2095 cm^{-1} to that

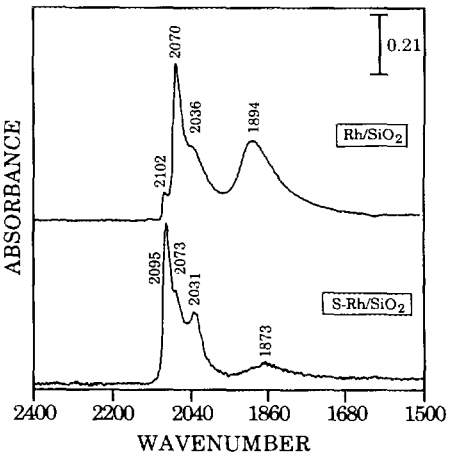

FIG. 1. CO adsorption on Rh/SiO_2 and S–Rh/SiO_2 at 303 K and 0.1 MPa.

at 2031 cm^{-1} is due to the combination of the 2095 cm^{-1} band with the symmetric stretching of the $Rh^+(CO)_2$ (gem-dicarbonyl). The 2095 cm^{-1} band has been assigned to $Rh^+(CO)$, a linear CO adsorbed on Rh^+ (*16, 29*). The CO coordinating with the Rh^+ is known to give bands at higher wavenumbers than CO adsorbing on Rh^0 (*26, 29–31*). Konishi *et al.* have found that the intensity of a CO band at 2090 cm^{-1} increases with sulfur coverage on Rh/SiO_2 and have suggested that the electronegative sulfur coordinates with the Rh, leaving a net positive charge on the Rh atom (*29*). The infrared spectra of CO chemisorbed on S–Rh/SiO_2 shown in Fig. 1 exhibit a higher intensity of linear CO and gem-dicarbonyl than our earlier study (*16*) due to the different sulfiding conditions, leading to different sulfur coverages on the catalyst.

Results of the pulse CO chemisorption on Rh/SiO_2 and S–Rh/SiO_2 at 303 K undertaken in the differential reactor are listed in Table 1. The amount of CO chemisorbed on Rh/SiO_2 is 16 times greater than that on S–Rh/SiO_2, while the overall integrated absorbance of adsorbed CO on Rh/SiO_2 at 0.1 MPa, shown in Fig. 1, is about two times greater than that of adsorbed CO on S–Rh/SiO_2. The difference between the amount of

TABLE 1

CO Chemisorption over Rh/SiO_2 and $S-Rh/SiO_2$

	Catalyst			
	Rh/SiO_2		$S-Rh/SiO_2$	
	0.1 MPa	1 MPa	0.1 MPa	1 MPa
Amount of CO adsorbed determined from pulse CO chemisorption in a differential reactor at 303 K (μmol/g)	16.36	—	1.07	—
$\bar{A}_{CO}$, IR absorption coefficients (cm/μmol)				
Linear CO	35		36	
Bridged CO	114		—	
μmol of CO/g-cat.[a] at 513 K and under hydroformylation conditions				
Linear CO	14.7	17.8	6.20	15.11
Bridged CO	11.73	11.60	1.50	4.17

[a] Estimated from $\bar{A}_{CO}$.

CO chemisorbed and the IR absorbances of adsorbed CO on Rh/SiO_2 and $S-Rh/SiO_2$ indicates that pulse CO chemisorption may underestimate the CO chemisorption capacity of the $S-Rh/SiO_2$ catalyst. Pulse CO chemisorption was conducted again in the IR reactor cell to determine the relationship between the integrated IR absorbances of chemisorbed CO and the amount of CO chemisorbed.

Figure 2 shows the IR spectra during the pulse CO chemisorption on Rh/SiO_2 in the IR reactor cell. The first pulse with 2.044 μmol of CO resulted in the development of the linear CO band at 2059 cm^{-1}, the bridged CO band at 1871 cm^{-1}, and the gem-dicarbonyl band at 2101 cm^{-1}. The IR absorbances of the CO bands following the first pulse corresponds to 0.27 μmol of CO chemisorbed. Table 1 lists the integrated IR absorption coefficients, $\bar{A}_{CO}$, for linear and bridged CO, which were calculated from the relation (*32*)

$$\bar{A}_{CO} = \frac{1}{\bar{C}_{CO}} \int_{\nu_l}^{\nu_u} A(\nu) d\nu$$

and the method developed by Rasband and Hecker (*33*). $\bar{C}_{CO}$ is the moles of CO chemisorbed/cross sectional area of the catalyst disk, and ν_l and ν_u are the lower and upper wavenumber bounds of the absorption bands in the above relation. The ratio of

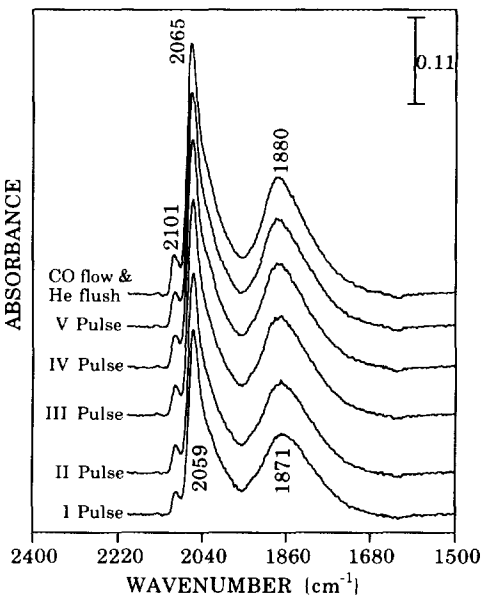

FIG. 2. Pulse CO chemisorption on Rh/SiO_2 at 303 K.

$\bar{A}_{CO}$ for bridged CO to linear CO is about 3, which is in agreement with that found in literature (*33*). However, the $\bar{A}_{CO}$ values determined here are higher than those reported (*32–35*). The error in calculating $\bar{A}_{CO}$ is estimated to be 20% due to the error compounded from the measurement of the size of the disk, integrated absorbances, and amount of CO chemisorbed. It has been reported that the $\bar{A}_{CO}$ for linear CO on Ru (*32*) and Pt (*34*) varies with CO coverage. In contrast, the $\bar{A}_{CO}$ for the gem-dicarbonyl on Rh/Al_2O_3 remains fairly constant (*35*). The $\bar{A}_{CO}$ for linear and bridged CO has been found to vary slightly with temperature (*33*). The $\bar{A}_{CO}$ determined at 303 K and 0.1 MPa may be used to estimate the quantity of CO chemisorption during the hydroformylation reaction.

Figure 2 shows sequential CO pulses leading to small increases in the integrated IR absorbances of the linear, bridged and gem-dicarbonyl bands, and the amount of CO chemisorbed. Exposure of the catalyst to 0.1 MPa of CO resulted in only a slight increase in the integrated absorbances of the linear CO band. The wavenumbers of the linear and bridged CO bands shifted from 2059 to 2065 cm^{-1} and from 1871 to 1880 cm^{-1}, respectively, during the entire process due to increasing CO coverage and dipole–dipole interactions (*36*).

Figure 3 shows the IR spectra during the pulse CO chemisorption on $S–Rh/SiO_2$ in the IR reactor cell. The first CO pulse resulted in the development of the linear CO band at 2061 cm^{-1}. The IR absorbance of the CO band following the first pulse corresponds to 0.03 μmol of CO chemisorbed. The integrated IR absorption coefficient, $\bar{A}_{CO}$, for linear CO on $S–Rh/SiO_2$ was consistent with that calculated for linear CO on Rh/SiO_2 as shown in Table 1. Pulsing CO sequentially resulted in a small quantity of CO chemisorbed and a small increase in the integrated IR absorbance of the linear CO band at 2061 cm^{-1} without any change in its wavenumber. Exposure of the $S–Rh/SiO_2$ catalyst to 0.1 MPa of CO resulted in significant spectral changes: (a) the emergence of a $Rh^+(CO)$ species, exhibiting the 2088 cm^{-1} band; (b) a threefold increase in the intensity of the linear CO band, accompanied by a shift in its wavenumber to 2071 cm^{-1}; and (c) the appearance of a weak gem-dicarbonyl band at 2029 cm^{-1} and a weak bridged CO band. The minor difference in the wavenumbers of adsorbed CO between Figs. 1 and 3 is due to slightly different sulfur coverages, although the same sulfiding conditions were employed. Prolonged exposure of the $S–Rh/SiO_2$ catalyst to CO resulted in small increases in the intensities of all the adsorbed CO bands.

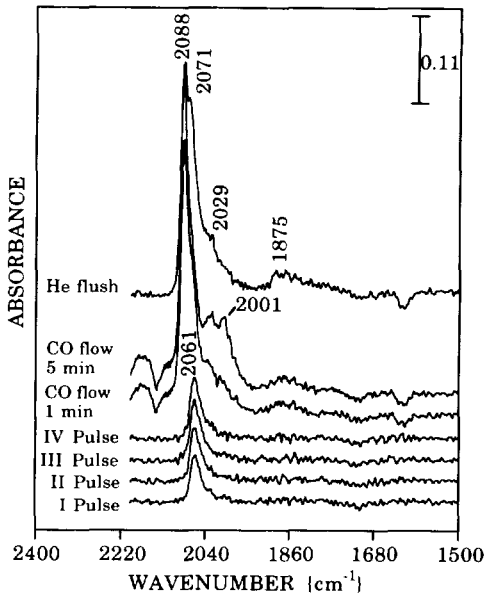

FIG. 3. Pulse CO chemisorption on $S–Rh/SiO_2$ at 303 K.

The significant increase in CO adsorption at 0.1 MPa of CO clearly indicates that saturated coverage of CO cannot be achieved by pulse CO chemisorption. The low CO uptake resulting from pulse CO chemisorption appears to be due to the slow adsorption of CO on the $S–Rh/SiO_2$. Thus, results of pulse CO chemisorption cannot be used to estimate the number of Rh surface atoms on the $S–Rh/SiO_2$ catalyst. The slow forma-

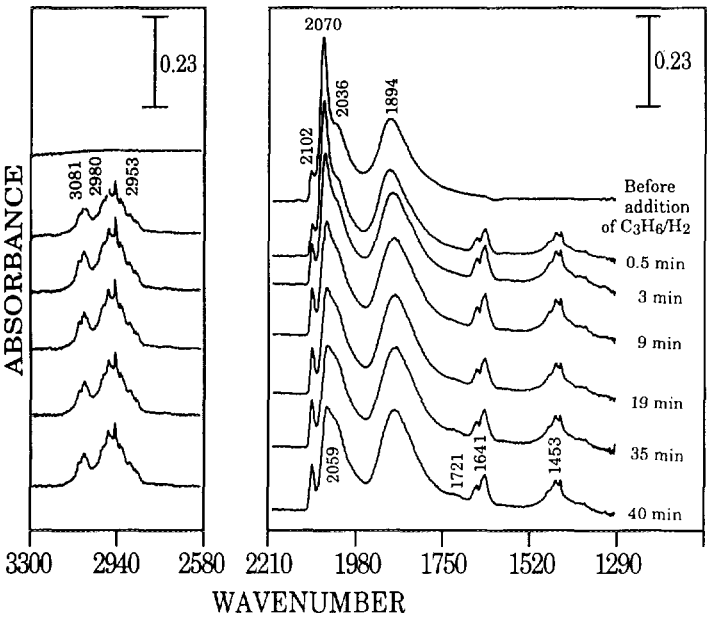

FIG. 4. Reaction of C_3H_6/H_2 with CO adsorbed on Rh/SiO_2 at 303 K and 0.1 MPa.

tion of $Rh^+(CO)$, linear CO, and gem-dicarbonyl has also been observed on S–Rh/SiO_2 in the presence of $CO : H_2 : C_3H_6 = 1 : 1 : 1$ at 0.1 MPa and 303 K. The greater dependence of the CO coverage on the partial pressure of CO, the slow uptake of CO and the slow formation of the chemisorbed CO bands in the presence of H_2 and C_3H_6 suggest that the equilibrium constant for CO chemisorption on S–Rh/SiO_2 could be smaller than that on Rh/SiO_2.

Reaction of Propylene and Hydrogen with CO Adsorbed on Rh/SiO_2

Figure 4 shows the IR spectra of the reaction of C_3H_6/H_2 with CO adsorbed at 303 K over Rh/SiO_2 as a function of time. The spectra taken just before admitting the C_3H_6/H_2 into the reactor showed linear CO at 2070 cm^{-1}, bridged CO at 1894 cm^{-1}, and the gem-dicarbonyl species at 2102 and 2036 cm^{-1}. Upon admitting 0.1 MPa of C_3H_6/H_2 (1 : 1) mixture, the intensity and wavenumber of the linearly adsorbed CO band at 2070 cm^{-1} decreased, while the intensity of the bridged CO increased with a decrease in the wavenumber. The decreased intensity of the linear CO band accompanied by a gradual downward shift in its wavenumber is attributed to a decrease in the concentration of adsorbed CO and the dipole–dipole coupling between adsorbed CO species (*36*). The gem-dicarbonyl bands at 2102 and 2036 cm^{-1} showed a slight increase in intensity. Bands at 1453, 1641, 2953, 2980, and 3081 cm^{-1} due to gaseous propylene (*37, 38*) showed slight variation in intensity with reaction time.

After 19 min of the isothermal batch reaction a small band emerged at 1721 cm^{-1}. This band can be assigned to butyraldehyde (*37, 38*). Distinction between *n*- and iso-butyraldehyde species could not be made from the IR spectra. Figure 5 highlights the change in IR intensity of adsorbed CO and aldehyde with respect to time. The initial decrease in the intensity of the linear CO band, accompanied by increases in the intensities of the bridged CO and gem-dicarbonyl bands suggests that a part of the linear CO may be converted to bridged CO and gem-dicarbonyl. The gradual decrease in the

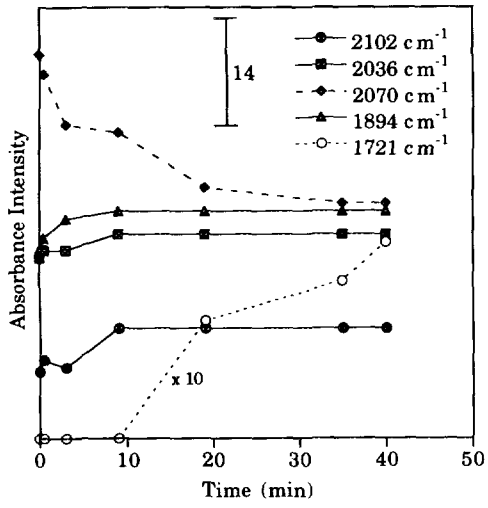

FIG. 5. Absorbance intensity vs time for Fig. 4.

intensity of the linear CO band after 10 min with the formation and a simultaneous increase in the intensity of the propionaldehyde band suggests that linear CO on Rh^0 sites is the active species that takes part in the formation of butyraldehyde on Rh/SiO_2.

Figure 6 shows the stability of the adsorbed CO species on Rh/SiO_2 in the presence of C_3H_6/H_2 and a small amount of propionaldehyde after the reaction of C_3H_6/H_2 with adsorbed CO. Increasing temperature to 333 K in the batch mode resulted in an increase in the aldehyde band and a rapid decrease in the intensities of the linear CO, bridged CO, and gem-dicarbonyl bands with the formation of CO_2, exhibiting bands at 2362 and 2338 cm^{-1}. The decrease in the intensities of the adsorbed CO bands is also accompanied by hydrogenation of propylene. Hydrogenation of propylene is evidenced by the disappearance of the propylene bands at 3081, 2953, 1641, and the 1453 cm^{-1} with the increase in intensity of the propane band at 2960 cm^{-1}, and formation of the 1470 cm^{-1} band. Adsorbed CO has an inhibiting effect on propylene hydrogenation. Increase in temperature to 423 K resulted in a decrease in the intensity of the linear CO, bridged CO, CO_2, and aldehyde bands. At temperatures above 393 K, a gradual increase in the intensity of bridged CO was observed with a slight decrease in the intensity of the CO_2 bands, suggesting con-

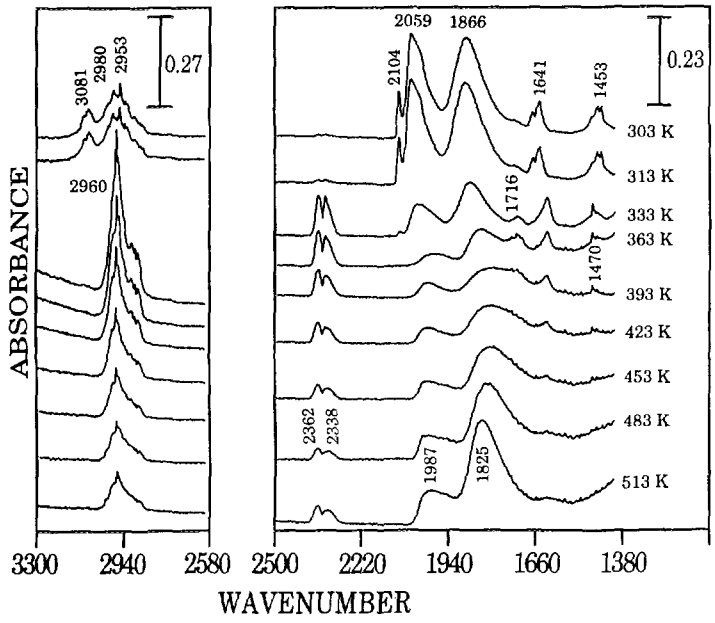

FIG. 6. Temperature-programmed reaction following reaction of C_3H_6/H_2 with CO adsorbed on Rh/SiO_2 at 303 K.

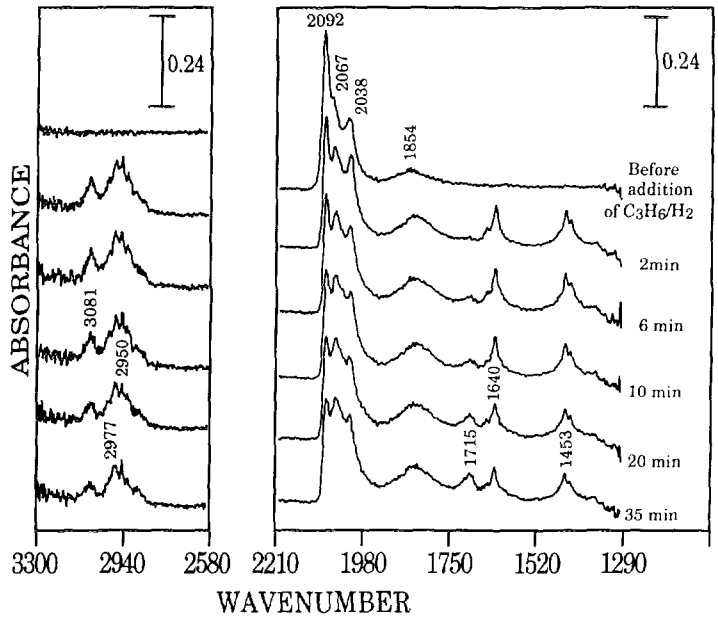

FIG. 7. Reaction of C_3H_6/H_2 with CO adsorbed on S–Rh/SiO_2 at 303 K and 0.1 MPa.

version of CO_2 to CO. Conversion of adsorbed CO_2 to adsorbed CO on Rh/SiO_2 in the presence of coadsorbed H_2 has also been reported (*39*).

Figure 7 shows the IR spectra of the reaction of C_3H_6/H_2 with CO adsorbed on sulfided Rh/SiO_2 at 303 K. The spectra taken prior to admitting the C_3H_6/H_2 mixture showed the Rh^+ (CO) band at 2092 cm^{-1}, the linear CO band at 2067 cm^{-1}, the asymmetric band of the gem-dicarbonyl, $Rh^+(CO)_2$, at 2038 cm^{-1}, and a weak bridged CO band at 1854 cm^{-1}. The addition of C_3H_6/H_2 to CO adsorbed on sulfided Rh/SiO_2 resulted in the following spectral development: (a) the appearance of the propylene bands at 1453, 1640, 2950, 2977, and 3081 cm^{-1}; (b) a gradual decrease in the intensity of the Rh^+(CO) band at 2092 cm^{-1} with reaction time; (c) the appearance of the butyraldehyde band at 1715 cm^{-1}, followed by an increase in its intensity; and (d) a slight initial increase in the intensities of the linear CO band at 2067 cm^{-1}, the bridged CO band at 1854 cm^{-1}, and the gem-dicarbonyl band at 2038 cm^{-1}.

Figure 8 shows the change in IR intensity with respect to time of adsorbed CO and aldehyde on S–Rh/SiO_2. The initial decrease in the intensity of the Rh^+(CO) band, accompanied by increases in the intensities of the linear CO, bridged CO, and gem-dicarbonyl bands suggests that a part of the

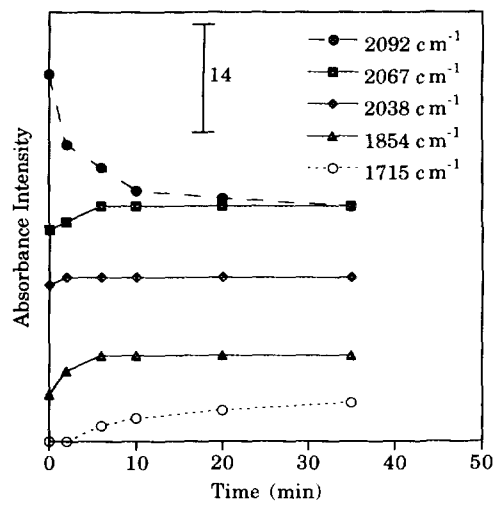

FIG. 8. Absorbance intensity vs time for Fig. 7.

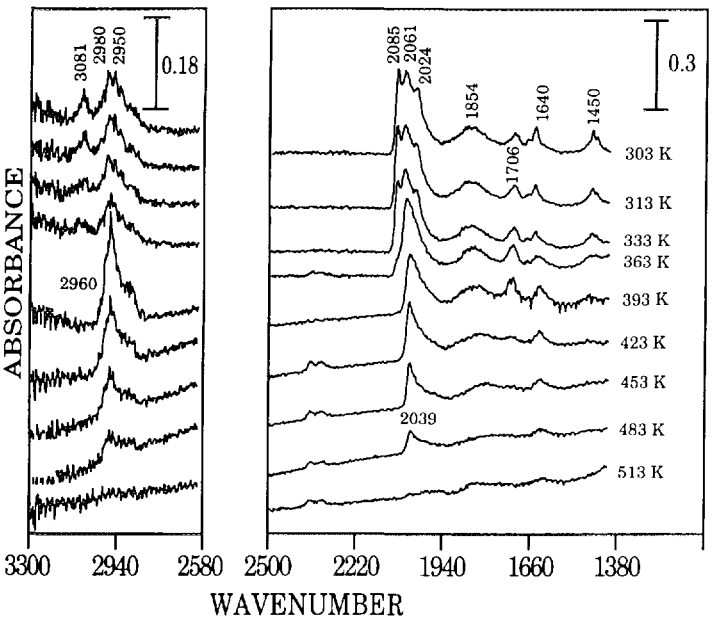

FIG. 9. Temperature-programmed reaction following reaction of C_3H_6/H_2 with CO adsorbed on S–Rh/SiO_2 at 303 K.

$Rh^+(CO)$ may be converted to linear CO, bridged CO, and gem-dicarbonyl. The increase in the intensity of the bridged CO band is most likely due to a small part of the sulfur desorbing. The intensity of the aldehyde band and its rate of formation on S–Rh/SiO_2 are greater than the corresponding band on Rh/SiO_2. The gradual decrease in the intensity of the $Rh^+(CO)$ band with the simultaneous increase in the intensity of the aldehyde band suggests that linear CO on Rh^+ sites is the active species that takes part in the formation of butyraldehyde on S–Rh/SiO_2. The possibility of the involvement of linear CO on Rh^0 in CO insertion on the S–Rh/SiO_2 catalyst may be ruled out because the linear CO band increased in intensity initially and remained constant during aldehyde formation.

Figure 9 shows the stability of the adsorbed CO species on S–Rh/SiO_2 in the presence of C_3H_6/H_2 and butyraldehyde after reaction of C_3H_6/H_2 with adsorbed CO on S–Rh/SiO_2. Increasing temperature to 393 K in the batch mode resulted in a complete removal of the $Rh^+(CO)$ and gem-dicarbonyl and a gradual decrease in the intensities of linear and bridged CO bands. A slight increase in the intensity of the 1706-cm^{-1} aldehyde band between 363 and 393 K was observed while $Rh^+(CO)$ was absent. This increase in the aldehyde band is accompanied by the decrease in the intensity of the linear CO band, suggesting that in the absence of the more reactive $Rh^+(CO)$ species the linear CO on Rh^0 undergoes CO insertion to form the aldehyde. The decrease in the intensities of the adsorbed CO bands is also accompanied by an increase in the hydrogenation of the propylene manifested by changes in the IR spectra in the 2580–3300 and 1400–1700 cm^{-1} regions. Adsorbed CO inhibits propylene hydrogenation on S–Rh/SiO_2; the required temperature for propylene hydrogenation on S–Rh/SiO_2 is higher than that on Rh/SiO_2. Further increase in temperature resulted in decreases in all the chemisorbed bands. Formation of CO_2 as a result of CO disproportionation is less on S–Rh/SiO_2 than on Rh/

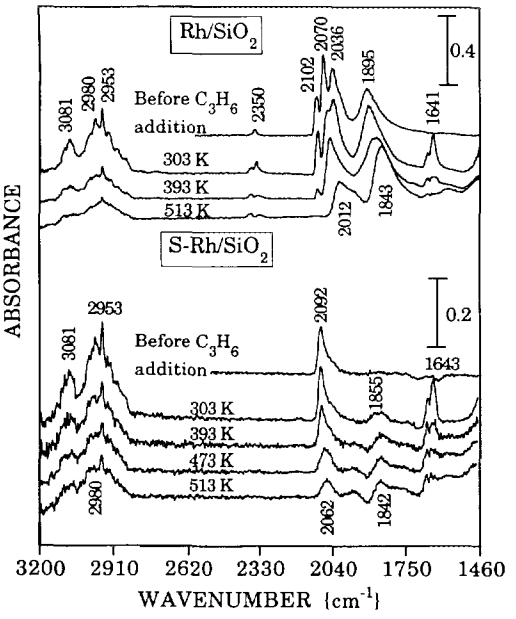

FIG. 10. Temperature-programmed reaction following reaction of C_3H_6 with CO adsorbed on Rh/SiO_2 and S–Rh/SiO_2 at 303K.

SiO_2. Comparison of Figs. 6 and 9 shows that CO_2 formation is reduced in the absence of bridged CO. Bridged CO may be the precursor for CO_2 formation via the disproportionation reaction.

The presence of H_2 is essential for the formation of butyraldehyde on both Rh/SiO_2 and S–Rh/SiO_2. The addition of C_3H_6 to adsorbed CO on Rh/SiO_2 and S–Rh/SiO_2 at 303 K resulted in desorption of a small amount of chemisorbed CO without formation of butyraldehyde even after a prolonged period of time, as shown in Fig. 10. Figure 10 shows the variation in intensity of adsorbed CO and propylene bands as a function of temperature following exposure of chemisorbed CO to C_3H_6 on Rh/SiO_2 and S–Rh/SiO_2. The absence of hydrogen limits the hydrogenation of propylene and adsorbed CO. The self-hydrogenation of propylene is manifested by the gradual decrease in the C=C vibration band at 1641 cm^{-1}. The dominant CO species at 513 K is bridged CO on Rh/SiO_2, while both linear and bridged CO are present on S–Rh/SiO_2 at 513 K. The 2062-cm^{-1} band on S–Rh/SiO_2 appears to be due to the downshift of the 2092-cm^{-1} band as its intensity decreases with temperature.

Propylene Hydroformylation on Rh/SiO_2 and Sulfided Rh/SiO_2

Figure 11 shows the spectra taken during steady-state propylene hydroformylation at 513 K and 0.1, 0.4, and 1 MPa on Rh/SiO_2 and S–Rh/SiO_2. Rates of product formation at 0.1 and 1 MPa corresponding to the IR spectra are shown in Table 2. Stable activity and selectivity were achieved 20 minutes after startup. The turnover frequency (TOF) for butyraldehyde formation in Table 2 has been calculated by dividing the rate of formation of butyraldehyde by the number of linear CO on the surface under reaction conditions estimated from $\overline{A}_{CO}$ and assuming that adsorbed CO is the most abundant species on the surface during the reaction. This assumption is based on the fact that the strong interaction of CO with the surface results in limiting C_3H_6 adsorption and hydrogenation inhibition. Rh surface atoms that chemisorb linear CO have been shown to be the active sites for CO insertion during ethylene hydroformylation (*16*) and propylene hydroformylation in this study.

The products of propylene hydroformylation consisted mainly of propane and small quantities of *n*- and iso-butyraldehyde. Intense bands due to linear CO at 2031 cm^{-1} and bridged CO at 1834 cm^{-1} and weak propylene bands in the vicinity of 2978 and 2953 cm^{-1} were observed during the steady-state reaction at 0.1 MPa on the Rh/SiO_2 catalyst. The aldehyde band could be overlapped with the bridged CO band. The bridged CO band under reaction conditions is significantly more intense than that under CO chemisorption conditions at 0.1 MPa and 303 K. A similar increase in the intensity ratio of bridged CO to linear CO has been observed for Ag–Rh/SiO_2 catalysts (*17*). The increase in the intensity ratio of bridged CO to linear CO suggests that the aggregation

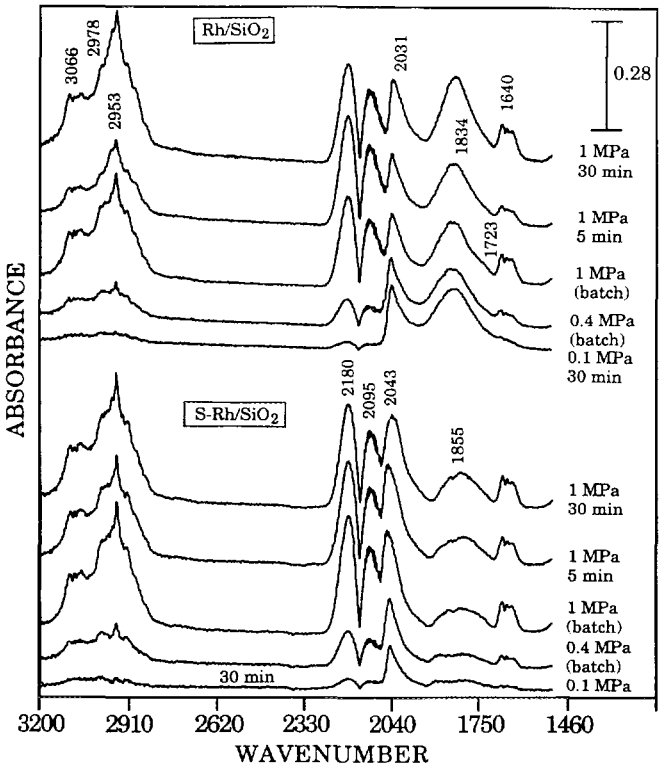

FIG. 11. Propylene hydroformylation on Rh/SiO_2 and$S–Rh/SiO_2$ at 513 K.

TABLE 2

Rate Data during Propylene Hydroformylation over Rh/SiO_2[a] and $S–Rh/SiO_2$ at 513 K

	Catalyst			
	Rh/SiO_2		$S–Rh/SiO_2$	
	0.1 MPa	1 MPa	0.1 MPa	1 MPa
Conv. of C_3H_6 (mol/kg · h)	4.15	12.79	0.66	1.90
TOF (min^{-1})[b] for formation of butyraldehyde	0.18	2.12	0.08	0.71
Product formation (mol/kg · h)				
n-C_3H_7CHO	0.12	1.54	0.02	0.35
iso-C_3H_7CHO	0.04	0.73	0.01	0.30
C_3H_8	3.75	10.13	0.55	1.20
Other hydrocarbons	0.23	0.39	0.08	0.05
Selectivity[c]				
(*n*-/iso-)	3.00	2.10	2.00	1.16
(Total butyraldehyde/C_3H_8)	0.04	0.22	0.05	0.54

[a] Average Rh crystallite size = 87 Å.
[b] Estimated from the number of surface Rh atoms that chemisorbed linear CO.
[c] Selectivity = (rate of formation of *A*)/(rate of formation of *B*).

of Rh crystallites leads to an increase in pair Rh atom sites for chemisorption of bridged CO. Both CO and H_2 have been found to promote agglomeration of Rh at temperatures above 423 K (*40*). The doublet at 2095 and 2180 cm^{-1} are due to gas-phase CO (*41*). Intensity of gas-phase CO bands increased with reaction pressure. The contour of the gas-phase CO bands under reaction conditions closely resembles those taken with a silica disk.

Increasing total pressure resulted in (a) an increase in the intensities of the linear CO band at 2031 cm^{-1} and hydrocarbon bands at 3066, 2978, 2953, and 1640 cm^{-1}; (b) a slight increase in the intensity of the bridged CO band at 1834 cm^{-1} followed by a pronounced increase in its intensity with reaction time; and (c) an enhancement in the rate of formation of all the products. The rates of formation for *n*- butyraldehyde, isobutyraldehyde, and propane were increased by a factor of 12, 18, and 2.7, respectively, suggesting that high pressure favors the formation of iso- butyraldehyde.

The spectra corresponding to 0.1 MPa on the sulfided catalyst showed the linear CO band at 2043 cm^{-1} and only a weak bridged CO band. The lower wavenumber of the linear CO band compared to 2061 cm^{-1} shown in Fig. 3 may be due to the low concentration of adsorbed CO in the presence of C_3H_6/H_2. The high wavenumber $Rh^+(CO)$ band is not present, indicating that the surface state of the catalyst at reaction condition is not the same as that at 303 K. Propane, *n*-butyraldehyde, and iso-butyraldehyde were the main products. Increasing pressure resulted in an increase in the intensities of the hydrocarbon bands, the linear and bridged CO bands, and the formation of butyraldehyde. The bridged CO band became more pronounced as reaction time increased, indicating that a part of the sulfur desorbs from the surface of the catalyst under a $CO/H_2/C_3H_6$ environment. Assuming that each surface sulfur atom blocks a bridged CO site, the increase in the intensity of bridged CO during the entire course of the reaction corresponds to the loss of 44% of the surface sulfur. X-ray fluorescence spectroscopy revealed that the bulk S content of the catalyst decreased by approximately 65%. Preliminary studies show that decreasing the sulfur coverage leads to an increase in the propylene hydrogenation activity of the catalyst.

A comparison of the rate data for the Rh/SiO_2 and sulfided Rh/SiO_2 catalysts shows that sulfur decreases the rate of overall propylene conversion and inhibits the formation of propane. The sulfur inhibition of propylene hydrogenation results in an enhancement of the aldehyde selectivity and in a decrease in the ratio of *n*- to iso-butyraldehyde selectivity. Increasing the reaction pressure from 0.1 to 1 MPa resulted in a greater increase in the intensity of the linear CO band and in the aldehyde selectivity over the $S–Rh/SiO_2$ catalyst than over the Rh/SiO_2 catalyst. The great dependence of linear CO intensity on pressure for the sulfided Rh catalyst from 0.1 and 1 MPa as compared to that of the Rh catalyst suggests that the adsorption equilibrium constant of linear CO could be smaller for $S–Rh/SiO_2$ than for Rh/SiO_2 under reaction conditions.

Propylene Hydrogenation on Rh/SiO_2 and Sulfided Rh/SiO_2

Fresh batches of reduced and sulfided catalysts were used for the propylene hydrogenation study. The IR spectra of steady-state hydrogenation on Rh showed intense propylene and propane bands (*41*). The $S–Rh/SiO_2$ catalyst exhibited weaker propane bands than the Rh/SiO_2 catalyst did. The products of the reaction are shown in Table 3. Stable activity was attained in 30 min. The reaction produced propane as the major product on both Rh and sulfided Rh. Sulfur decreased the rate of formation of propane by two orders of magnitude. The TOF has been calculated using the Rh surface atoms estimated from $\overline{A}_{CO}$ at 303 K.

DISCUSSION

The interactions of CO on supported Rh catalysts have been widely studied (*22–31*,

TABLE 3

Rate Data during Propylene Hydrogenation over Rh and S–Rh Catalysts at 513 K and 0.1 MPa

	Catalyst	
	Rh/SiO_2	$S–Rh/SiO_2$
Conv. of C_3H_6(mol/kg · h)	341.17	5.93
TOF (min^{-1})[a]	215.14	30.40
Product formation (mol/kg · h)		
CH_4	0.38	—
C_2H_4	0.02	0.01
C_2H_6	0.65	0.07
C_3H_8	339.97	5.87
C_4H_8	0.01	—
C_4H_{10}	0.14	—

[a] Surface Rh atoms calculated from $\bar{A}_{CO}$ at 303 K and 0.1 MPa.

42–44). The types of CO adsorbed on the Rh surface are closely related to the structure and the chemical environment of the Rh surface. It has been well established that the reduced Rh crystallite surface adsorbs CO as linear and bridged CO, and oxidized Rh contains mainly isolated Rh^+ sites chemisorbing CO as the gem-dicarbonyl (*16, 17, 22–31, 42–45*). Gem-dicarbonyl can also be generated by oxidative disruption of the Rh crystallites involving OH groups of the support and carbon monoxide (*44, 45*).

Adsorbed sulfur inhibits the formation of the bridged CO band on Rh/SiO_2. The inhibition of the bridged CO species by the addition of sulfur is due to the disruption of adjacent Rh^0 sites that are necessary for adsorbing CO in the bridged form. The intense 2095-cm^{-1} band on $S–Rh/SiO_2$ is partly due to contribution from the band due to the symmetric vibration of the gem-dicarbonyl species adsorbed on Rh^+ sites. The formation of $Rh^+(CO)$ on $S–Rh/SiO_2$ requires higher CO pressure than that of $Rh^+(CO)_2$ on Rh/SiO_2. The distinction between Rh^+ sites that chemisorb linear CO and Rh^+ sites that chemisorb gem-dicarbonyl remains unclear.

The bulk S/Rh atomic ratio of the $S–Rh/SiO_2$ catalyst was determined to be 0.04 using XRF, which corresponds to a sulfur coverage (Θ_s) of 55% determined from CO chemisorption. The low bulk S/Rh atomic ratio and the high sulfur coverage suggest that the sulfidation occurs primarily on the surface of the catalyst under the given conditions. When low concentrations of H_2S are used for sulfiding, bulk sulfides are unstable and surface sulfides are formed. (*46*).

A comparison of the rate of formation of the aldehyde from the reaction of adsorbed CO with propylene and hydrogen at 303 K shows that Rh^+ sites on the $S–Rh/SiO_2$ are more active for the formation of butyraldehyde (CO insertion) than Rh^0 sites on the Rh/SiO_2. Previous studies on ethylene hydroformylation on Rh/SiO_2 (*16*) have also demonstrated that the Rh^+ site on the oxidized Rh is more active for CO insertion into the adsorbed ethyl species than the Rh^0 site on the reduced Rh catalyst. However, the activity of linear CO on Rh^+ sites on $S–Rh/SiO_2$ for ethylene hydroformylation (CO insertion) at 303 K is significantly lower on sulfided Rh/SiO_2 than that on the oxidized Rh/SiO_2 as a result of the sulfur inhibition of ethylene adsorption. Higher temperatures are required to initiate adsorption of ethylene on the sulfided Rh catalyst. In contrast, propylene hydroformylation from the reaction of C_3H_6/H_2 with adsorbed CO on $S–Rh/SiO_2$ can take place at room temperature.

In homogeneous hydroformylation the rate of aldehyde formation from olefin hydroformylation decreases with increasing alkene substitution; more alkyl groups attaching to the carbon atom with the double bond result in lower rates of aldehyde formation (*2–4, 10*). The rate of ethylene hydroformylation is higher than that of propylene hydroformylation on the same metal complex catalyst. The same trend is observed for steady-state ethylene and propylene hydroformylation on both Rh/SiO_2 and $S–Rh/SiO_2$ (*16*).

It is still unclear why C_3H_6/H_2 is more reactive toward adsorbed CO leading to aldehyde formation on the $S–Rh/SiO_2$ than

C_2H_4/H_2 at 303 K. Little is known about how olefins coadsorb with CO or other molecules on the surface of supported metal catalysts. Adsorption of C_2H_4 and C_3H_6 on Rh(100) single crystal shows that C_2H_4 adsorbs on Rh(100) forming ethylidyne and C_3H_6 forms both propylidyne and ethylidyne species at 303 K (*47, 48*). Adsorbed CO and sulfur inhibit the formation of adsorbed ethylidyne species (*47*). Due to the intense gas-phase bands in the 2800–3200 cm^{-1} region and the infrared bands for hydrocarbon fragments below 1300 cm^{-1} blocked by the CaF_2 windows and SiO_2, we are not able to obtain any information on the adsorbed state of the olefin from our studies.

The effect of sulfur on steady-state propylene hydroformylation has been identified as (i) a decrease in the CO conversion, (ii) a suppression of hydrogenation activity, and (iii) a decrease in the concentration of bridged CO and shifting of the linear CO to a higher wavenumber under reaction conditions. The effect of sulfur on the catalytic reaction has often been interpreted by (i) geometric site blocking by adsorbed sulfur, and (ii) electronic interactions of the surface sites with adsorbed sulfur (*48, 49*). The geometric site-blocking of sulfur results in the blocking of bridged CO sites that have been shown to be inactive for CO insertion (*16, 19*). Therefore, increasing the ratio of linear to bridged CO sites should result in an enhancement of the CO insertion activity and thus improve aldehyde selectivity. Electronic interactions of sulfur with surface Rh result in the formation of Rh^+ sites, which have been demonstrated to be more active for CO insertion than Rh^0 sites. Nevertheless, the lack of a strong IR band for the high wavenumber $Rh^+(CO)$ under reaction conditions suggests that Rh^+ sites may not be present in large quantities under steady-state hydroformylation conditions at 513 K and 0.1–1 MPa. The temperature-programmed study in Fig. 9 shows that linear CO on Rh^+ desorbs completely at temperature above 363 K in the presence of H_2; the study in Fig. 10 shows that $Rh^+(CO)$ shifts to 2062 cm^{-1} at 513 K in the absence of H_2. An earlier temperature-programmed study on $RhCl_3/SiO_2$ has shown that linear CO on Rh^+ is stable at 573 K (*50*). Since $Rh^+(CO)$ can be present at 513 K, the disappearance of the high-wavenumber $Rh^+(CO)$ on S–Rh/SiO_2 suggests that the reduction of Rh^+ takes place under reaction conditions. Although the exact nature of the sulfided Rh surface under reaction conditions remains to be investigated, a higher wavenumber of linear CO at 2043 cm^{-1} on the sulfided Rh/SiO_2 compared to that of linear CO at 2031 cm^{-1} on the Rh/SiO_2 under hydroformylation conditions confirms that the Rh on S–Rh/SiO_2 is more electropositive than that on Rh/SiO_2.

The main difference between homogeneous and heterogeneous hydroformylation is the high hydrogenation activity of heterogeneous catalysts (*4, 16, 29, 51, 52*). The high hydrogenation activity of heterogeneous metal surfaces has been attributed to ease of dissociation of dihydrogen and access to a pair of vacant sites on the metal surface (*29*). In contrast, the site for hydrogen-oxidative addition in homogeneous hydroformylation catalysts is located at a single Rh center atom of the mononuclear carbonyl where hydrogen oxidative addition is slow compared to other reaction steps in hydroformylation (*53*).

Adsorbed sulfur inhibits hydrogen chemisorption at 303 K and high sulfur coverage also poisons olefin hydrogenation (*54*). However, at the hydroformylation conditions, a part of the sulfur desorbs leading to a recovery in the hydrogenation activity. In addition, most metal sulfides exhibit hydrogenation activity at temperatures below 473 K and 0.1 MPa (*54*). A comparison of our results with Rh carbonyl catalyzed reactions shows that the hydrogenation activity of sulfided Rh remains much higher than that of the Rh carbonyl.

The principle of homogeneous catalysis can be used in understanding catalysis on surfaces (*55, 56*). The effect of additives on the active site has been considered to resem-

ble the effect of ligands on the catalytic properties of the metal center of the metal carbonyl in homogeneous catalysis (*2, 55, 56*). The additives and ligands affect the activity and selectivity of reactions via their geometric and/or electronic effects. An increase in the formation of *n*- butyraldehyde during hydroformylation over alkyl-phosphine (PR_3) Co and Rh carbonyls as compared to unmodified carbonyls is attributed to the large size of the PR_3 ligands. The bulky size of alkyl-phosphine ligands crowds the environment of the Rh center atom of mononuclear complexes. This inhibits the isomerization of linear olefins to form secondary alkyl groups and only allows the migratory insertion of CO to occur into the linear alkyl groups producing linear aldehyde.

The steric (geometric) effect of ligands on the normal and iso-aldehyde selectivity may be employed to explain the geometric effect of adsorbed sulfur on the formation of iso-butyraldehyde on the catalyst surface. Rh-pair sites necessary for bridged CO chemisorption are blocked and protruding (corner) Rh atoms or ions are created by sulfur chemisorption on Rh/SiO_2 (*29*). These isolated corner sites should be favorable for the formation of iso-butyraldehyde (as shown by a decrease in the *n*- to iso-butyraldehyde ratio for $S–Rh/SiO_2$ in Table 2) due to the less crowded environment of Rh^+ sites on $S–Rh/SiO_2$ than the Rh^0 sites on reduced Rh/SiO_2. Such a spacious environment would facilitate isomerization of propyl groups before CO insertion.

The increased size of the phosphine ligand enhances the selectivity of the linear aldehyde, and increases hydrogenation activity, but decreases the overall hydroformylation activity (*10*). Although it is not clear how important the electronic properties of the phosphine ligand are in affecting the *n*-/iso-aldehyde selectivity (*2, 4, 10*), phosphine ligands are better σ donors and weaker π acceptors than CO, and consequently strengthen the Rh–CO bond by stronger electron back donation. The electron-donating phosphine ligands stabilize the phosphine Co or Rh complexes, alter the rate-determining step, and cause an increase in hydrogenation and a decrease in the CO insertion activity (*1–4, 10*). In contrast, the electronegative sulfur, which is a strong electron acceptor, induces the neighboring Rh to carry a positive charge resulting in an increase in the CO insertion activity and a decrease in the hydrogenation activity. Although there is an inverse correlation between the effect of electron-donating phosphine ligands on Rh complexes and the effect of electronegative sulfur on $S–Rh/SiO_2$, further study is needed to provide insight into the relationship between the hydroformylation on metal complexes and supported metals.

CONCLUSIONS

CO adsorption on 3 wt% Rh/SiO_2 produced linear CO, bridged CO, and the gem-dicarbonyl at 303 K and 0.1 MPa. Sulfidation of Rh/SiO_2 resulted in the disruption of the bridged CO sites and in the formation of Rh^+ sites that chemisorb linear CO, $Rh^+(CO)$. High CO pressure is required to form $Rh^+(CO)$ on the $S–Rh/SiO_2$ catalyst. $Rh^+(CO)$ is removed from the $S–Rh/SiO_2$ in the presence of C_3H_6/H_2 at temperatures above 363 K, while it remains stable in the presence of C_3H_6 at 513 K. Rh^+ that chemisorbs linear CO is more active for CO insertion producing butyraldehyde from the reaction with C_3H_6/H_2 than Rh^0 that adsorbs linear CO at 303 K. Bridged CO appears to be inactive for the reaction at 303 K. Under 513 K and 0.1–1 MPa, $S–Rh/SiO_2$ which has a higher ratio of linear CO to bridged CO showed a higher hydroformylation selectivity than Rh/SiO_2 which has a lower linear CO/bridged CO ratio. Sulfur increased the iso-/*n*-butyraldehyde ratio at 513 K and 0.1–1 MPa. The increase in the ratio of iso- to *n*-butyraldehyde may be explained in light of the effect of phosphine ligands in homogeneous hydroformylation.

ACKNOWLEDGMENTS

We acknowledge the partial support of this research by the U.S. Department of Energy (DE-FG-87PC79923) and the Research Challenge Program of the Ohio Board of Regents.

REFERENCES

1. Kiem, W., "Catalysis in C_1 Chemistry." Reidel, Boston, 1983.
2. Masters, C., "Homogeneous Transition-Metal Catalysis—A Gentle Art," p. 102. Chapman & Hall, New York, 1981.
3. Parshall, G. W., "Homogeneous Catalysis." Wiley, New York, 1980.
4. Piacenti, F., and Pino, P., *in* "Organic synthesis via Metal Carbonyls" (I. Wender and P. Pino, Eds.). Wiley, New York, 1977.
5. Wender, I., Sternberg, H. W., and Orchin, W., *in* "Catalysis" (P. H. Emmett, Ed.), Vol. 5, p. 73 Reinhold, New York, 1957.
6. Pruett, R. L., *J. Chem. Edu.* **63**(3), 196 (Mar. 1986).
7. Rode, E. J., Davis, M. E., and Hanson, B. E., *J. Catal.* **96,** 563 (1985).
8. Arai, H., *J. Catal.* **51,**135 (1978).
9. Pittman, C. U., Jr., and Smith, L. R., *J. Am. Chem. Soc.* **97,** 1749 (1975).
10. Cornils, B., *in* "New Syntheses with Carbon Monoxide" (J. Falbe Ed.). Springer-Verlag, New York, 1980.
11. Takahashi, N., and Kobayashi, M., *J. Catal.* **85,** 89 (1984).
12. Naito, S., and Tanimoto, M., *J. Catal.* **130,** 106 (1991).
13. Kuntz, E. G., *Chemtech*, 571 (Sept. 1987).
14. Arhancet, J. P., Davis, M. E., Merola, J. S., and Hansen, B. E., *J. Catal.* **121,** 327 (1990).
15. Frankel, E. N., Thomas, F. L., Rohwedder, W. K., *Ind. Eng. Chem. Prod. Res. Dev.* **12,** 47 (1973).
16. Chuang, S. S. C., and Pien, S. I., *J. Catal.* **135,** 618 (1992).
17. Chuang, S. S. C., and Pien, S. I., *J. Catal.* **138,** 536 (1992).
18. Takahashi, N., Mijin, A., Suematsu, H., Shinohara, S., and Matsuoka, H., *J. Catal.* **117,** 348 (1989).
19. Chuang, S. S. C., and Pien, S. I., *J. Mol. Catal.* **55,** 12 (1989).
20. Ichikawa, M., *J. Catal.* **59,** 67 (1979).
21. Sarkany, J., and Gonzalez, R. D., *J. Catal.* **76,** 75 (1982).
22. Underwood, R. T., and Bell, A. T., *J. Catal.* **111,** 325 (1988).
23. Yates, J. T., Jr., Duncan., M. T., and Vaughan, R. W., *J. Chem. Phys.* **71,** 3908 (1979).
24. Kesroui, S., Oukaci, R., and Blackmond, D. G., *J. Catal.* **105,** 432 (1987).
25. Yang, A. C., and Garland, C. W., *J. Phys. Chem.* **61,** 1504 (1957).
26. Li, Y. E., and Gonzales, R. D., *J. Phys. Chem.* **92,** 1589 (1988).
27. Yates, J. T., Jr., Duncan, T. M., Worley, S. D., and Vaughan, R. W., *J. Chem. Phys.* **70,** 1219 (1979).
28. Solymosi, F., Tombacz, I., and Kocsis, M., *J. Catal.* **75,** 78 (1982).
29. Konishi, Y., Ichikawa, M., and Sachtler, W. M. H., *J. Phys. Chem.* **91,** 6286 (1987).
30. Worley, S. D., Rice, C. A., Mattson, G. A., Curtis, C. W., Guin, J. A., and Tarrer, A. R., *J. Chem. Phys.* **76,** 20 (1982).
31. Rice, C. A., Worley, S. D., Curtis, C. W., Guin, J. A., and Tarrier, A. R., *J. Chem. Phys.* **74,** 6487 (1981).
32. Winslow, P., and Bell, A. T., *J. Catal.* **86,** 158 (1984).
33. Rasband, P. B., and Hecker, W. C., *J. Catal.* **139,** 551 (1993).
34. Heyne, H., and Tompkins, F. C., *Trans. Faraday Soc.* **63,** 1274 (1967).
35. Cavanagh, R. R., and Yates, J. T., Jr., *J. Chem. Phys.* **74**(1), 4150 (1981).
36. Stoop, F., Toolenar, F. J. C., and Ponec, V., *J. Catal.* **73,** 50 (1982).
37. Colthup, N. B., Daly, L. H., and Wiberly, S. E., "Introduction to Infrared and Raman Spectroscopy." Academic Press, New York, 1990.
38. Hair, M. L., "Infrared Spectroscopy in Surface Chemistry." Dekker, New York, 1967.
39. Solymosi, F., and Knozinger, H., *J. Catal.* **122,** 166 (1990).
40. Solymosi, F., and Paztor, M., *J. Phys. Chem.* **90,** 5312 (1986).
41. Srinivas, G., Master's Thesis, University of Akron, 1991.
42. Yates, D. J. C., Murrel, L. L., Prestridge, E. B., *J. Catal.* **57,** 41, (1979).
43. Yates, J. T., Jr., and Kolasinski, K., *J. Chem. Phys.* **79,** 1026 (1983).
44. Solymosi, F., and Paztor, M., *J. Phys. Chem.* **89,** 4789 (1985).
45. Basu, P., Panayotov, D., and Yates, J. T., Jr., *J. Am. Chem. Soc.* **110,** 2074 (1988).
46. Bartholomew, C. H., Agrawal, P. K., and Katzer, J. R., *Adv. Catal.* **31,** 135 (1982).
47. Slavin, A. J., Bent, B. E., Kao, C.-T., and Somorjai, G. A., *Surf. Sci.* **206,** 124 (1988).
48. Bent, B. E., Mate, C. M., Crowell, J. E., Koel, B. E., and Somorjai, G. A., *J. Phys. Chem.* **91,** 1493 (1987).
49. Oudar, J., *in* "Deactivation and Poisoning of Catalysis" (J. Oudar and H. Wise, Eds.), p. 51. Dekker, New York/Basel, 1985.
50. Chuang, S. S. C., Srinivas, G., and Mukherjee, A., *J. Catal.* **139,** 490 (1993).

51. Elschenbroich, C., and Salzer, A., "Organometallics—A Concise Introduction." VCH Publishers, New York, 1989.
52. Marko, L., *in* "Aspects of Homogeneous Catalysis" (R. Ugo, Ed.), Vol. 2, p. 4 Reidel, Boston, 1974.
53. Gates, B. C., "Catalytic Chemistry." Wiley, New York, 1992.
54. Mitchell, P. C. H., *in* "Catalysis," Vol. 1. The Chemical Society, Burlington House, London 1977.
55. Muetterties, E. L., Rhodin, T. N., Band, E., Brucker, B. F., and Pretzer, W. R., *Chem. Rev.* **79**(2), 91 (Apr. 1979).
56. Sachtler, W. M. H., *in* "Proceedings of the 8th International Congress on Catalysis, Berlin, 1984," Vol. 1. Verlag Chemie, Deerfield Beach, Florida, 1984.